Magmatic-metering controls the stopping and restarting of eruptions

Roozbeh Foroozan,[1] Derek Elsworth,[1] Barry Voight,[2] and Glen S. Mattioli[3]

Received 23 December 2010; revised 24 January 2011; accepted 28 January 2011; published 11 March 2011.

[1] We use time-series of magma efflux and GPS-derived surface deformation observations to constrain the transfer of compressible magma within the crustal plumbing of the Soufrière Hills volcano for three cycles of effusion and pause. Our system model has two vertically-stacked spherical chambers. Deep melt supply to the system is constrained to be continuous and steady, yielding a rate of 1.2 m^3/s, which fixes the geometry of the dual interconnected chambers to depths of about 5 and 19 km. The eruptive volume change of the shallow chamber is in-phase and an order of magnitude smaller than the deep chamber. Significantly, the shallow chamber seems to control the periodic system behavior: surface magma efflux resumes when the shallow chamber reinflates to its initial threshold pre-eruptive volume (triggering re-opening of an eruptive feeder dike), and ceases when it has lost 14–22 Mm^3 (10^6 m^3) of its volume (sealing the conduit and staunching magma flow). These observations are consistent with eruption re-initiation and re-cessation controlled by magma overpressure thresholds. **Citation:** Foroozan, R., D. Elsworth, B. Voight, and G. S. Mattioli (2011), Magmatic-metering controls the stopping and restarting of eruptions, *Geophys. Res. Lett.*, *38*, L05306, doi:10.1029/2010GL046591.

1. Introduction

[2] Continuous and highly resolved geodetic and efflux records are available for very few volcanoes. The recent eruption at Soufrière Hills (SHV) volcano on Montserrat, WI [*Mattioli et al.*, 2010; *Mattioli and Herd*, 2003] is an exception, providing an invaluable window into deep processes contributing to stratovolcano behavior. We constrain magma efflux with wide-aperture geodetic GPS observations (Figure 1, left) to supplement a well-documented effusion record [*Wadge et al.*, 2010], and use these to explore the role of deeply sourced fluxes on short-term eruption periodicity. We apply this method to recent activity at SHV where the phreatic activity began in July 1995 following several years of seismic unrest. An andesite dome grew continuously in extrusive episode 1 from November 1995 to ~10 March 1998, followed by a period of an eruptive pause with mild explosive activity [*Wadge et al.*, 2010] that ended in November 1999. This cycle, of an active lava dome extrusion episode followed by a pause, was repeated a second time, with extrusive episode 2 starting in December 1999 and continuing to mid-July 2003, followed by a pause lasting until October 2005. Extrusive episode 3 commenced in October 2005 and ended March 2007 [*Loughlin et al.*, 2010], followed by a pause lasting until July 2008. Thereafter there were two additional, but short extrusive episodes, 4 (from July 2008 to January 2009) [*Wadge et al.*, 2010] and 5 (from October 2009 to February 2010), which suggest changes in fundamental periodicity and flow dynamics after the first three cycles. We focus here on the consistent behaviors of the first three cycles.

[3] The restriction of volcano-seismicity since magma breakthrough in 1995 to <5 km depth, the stability of crystal phases at pressures of ~130 MPa, and inversion of early GPS data (1995 to 1997) were consistent with a magma chamber top at roughly 5 km depth [*Aspinall et al.*, 1998; *Barclay et al.*, 1998; *Miller et al.*, 2010], and this has been confirmed by recent seismic tomography [*Voight et al.*, 2010a]. Clots of basalt mixed in the erupted andesite indicate a deeper supply of mafic magma [*Annen et al.*, 2005; *Murphy et al.*, 2000] and some crystal phases suggest a connected deep chamber at >10 km [*Devine et al.*, 2003]. Geodetic data have provided further support for deep storage [*Mattioli et al.*, 2010], whether interpreted as single chambers of various shapes [*Mattioli et al.*, 2010; *Voight et al.*, 2008, 2010b], or interconnected chambers in shallow (~5 km) and relatively deep (>12 km) crust [*Elsworth et al.*, 2008]. *Voight et al.* [2010b] proposed a vertically-elongated chamber of complex shape idealized as a prolate ellipsoid, to accommodate both mineralogical constraints indicating shallow storage, and geodetic constraints inferring a deeper mean-pressure source; this chamber was assumed stratified with upper parts compressible due to exsolved gas phases, and fed at the base by deep influx. Philosophically the distinction between this model, and a two-chamber model with synchronous responses and a compressible upper chamber, may be slight, and there are some computational advantages for the latter. *Foroozan et al.* [2010] showed that the deformations of GPS stations located near or far from the volcano could not be explained with a single spherical pressure source. The significant cumulative volume of the eruption (~1.0 km^3, from 1995 to 2009) [*Wadge et al.*, 2010] and its continuity and chemical consistency, coupled with detailed observations of co-eruptive ground displacements suggests a voluminous upper magma source of several to tens km^3 [*Voight et al.*, 2006; 2010b]. When taken together, these observations constrain our proposed model of two vertically-stacked magma chambers. In contrast to *Elsworth et al.* [2008] we invert GPS data from 6 to 13 stations (versus 4 previously) to define chamber geometry and constrain these for new efflux data [*Wadge et al.*, 2010]. We then

[1]Department of Energy and Environmental Engineering, G3 Center and EMS Energy Institute, Pennsylvania State University, University Park, Pennsylvania, USA.
[2]Department of Geosciences, Pennsylvania State University, University Park, Pennsylvania, USA.
[3]Department of Earth and Environmental Sciences, University of Texas at Arlington, Arlington, Texas, USA.

0094-8276/11/2010GL046591

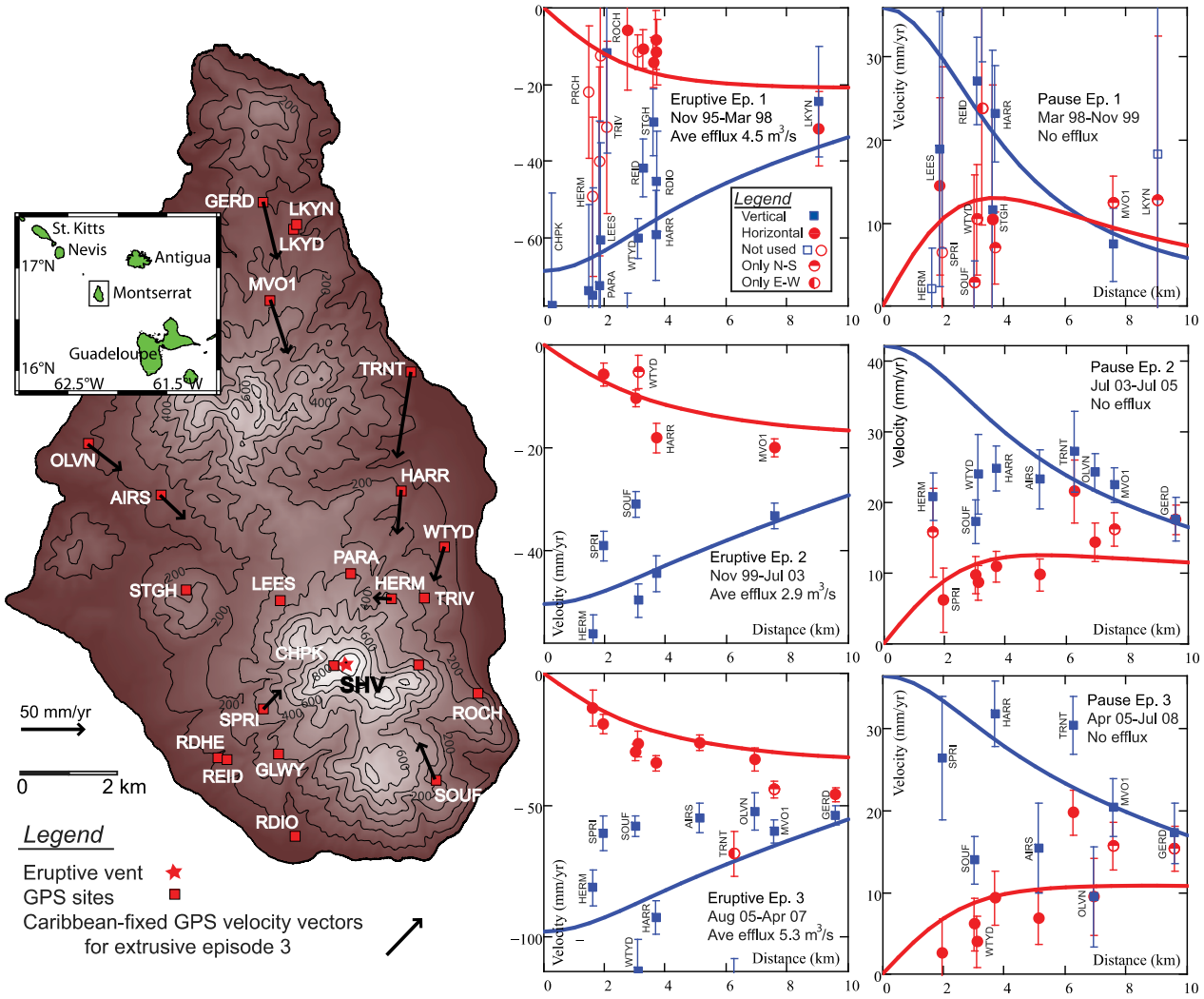

Figure 1. (left) Map of Soufriere Hills volcano. (right) Inversion results for dual Mogi sources at 5 km and 19 km. Radial (red) and vertical (blue) velocities (mm/yr) versus radial distance from the conduit (km). Error bars are one standard variation. Outlier measurements have open symbols.

use a compressible magma phase [*Huppert and Woods*, 2002] (versus incompressible previously) to define metered volumes of the upper chamber that control the periodicity of eruption.

2. Data

[4] This analysis inverts geodetic data from GPS stations [*Mattioli et al.*, 2010] in each eruptive/pause phase distributed around the island with the closest station ~1.6 km from the volcanic vent and the furthest ~9.6 km (Figure 1). We recover average and standard deviation of deformation rates within each of the episodes of eruption and pause. Consistently these measurements (with one exception in the first pause episode: SOUF) represent ground subsidence during periods of eruption and uplift during pause (Figure 1, right). Consistent with surface deformation above a deforming chamber, vertical velocities decrease radially outwards from the chamber center and horizontal velocities increase from zero above the chamber, through a peak and then toward zero in the far-field. Estimates of surface efflux from the conduit provide average efflux rates (Figure 1, right) in each of the three periods of eruption and three periods of pause [*Wadge et al.*, 2010].

3. Methods

[5] We treat the system as dual vertically-stacked chambers pierced by a vertical conduit that connects a deep-crustal supply zone with the effusing vent of SHV [*Elsworth et al.*, 2008]. The solid earth system is assumed inhomogeneously elastic with the surface deformations resulting from each embedded chamber represented by spherical point pressure source [*Mogi*, 1958; hereafter Mogi source]. This approach results in homogeneous-model depths modified by $D' = kD$, where D' is "apparent depth" of pressure source from elastically homogeneous inversion and D is actual depth in the inhomogeneous medium, and k is a correction factor. For the shallow chamber we take k as 0.73 [*Foroozan et al.*, 2010]; for the deeper chamber k is uncertain due to our limited knowledge of modulus structure >8 km depth under SHV, and we use the provisional value $k \sim 1$.

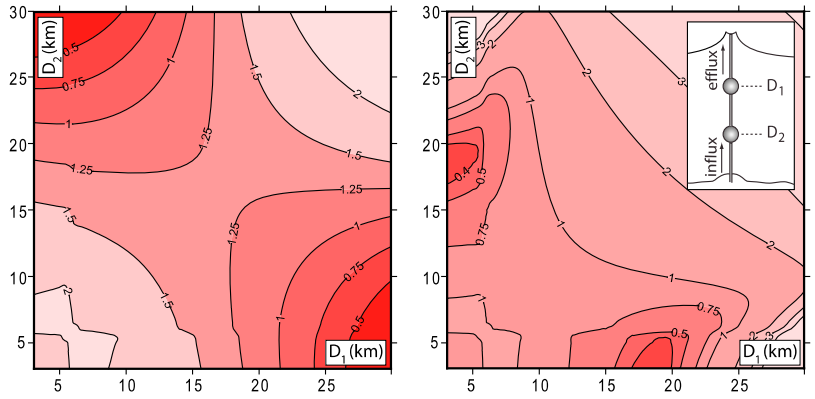

Figure 2. (left) Deep chamber mean influx (m_3/s) and (right) coefficient of variation of the deep chamber influx for the combined six successive episodes of activation and repose. The axes are the respective apparent depths (km) for the dual Mogi sources.

[6] In contrast to *Elsworth et al.* [2008], the infilling magma is assumed slightly compressible with the exsolved gas content controlling its effective modulus. In the compressibility calculations [*Huppert and Woods*, 2002], we assume andesite in both chambers. The exsolved volatile (water) content follows Henry's law [*Burnham*, 1975; *Melnik and Sparks*, 1999]. Further assumptions are a melt water content of 5% [*Barclay et al.*, 1998; *Murphy et al.*, 2000], a volumetric crystal fraction of 40–60% [*Devine et al.*, 1998; *Murphy et al.*, 2000], and a temperature of 850 C for andesite magma [*Devine et al.*, 2003; *Murphy et al.*, 2000]. Pressure is lithostatic assuming constant wallrock density of 2600 kg/m^3. The densities of crystals and melt are considered constant at 2700 kg/m^3 and 2300 kg/m^3 [*Costa et al.*, 2007; *Melnik and Sparks*, 1999] and the gas phase follow the ideal gas law.

[7] We evaluate rates of magma transport through the crustal column and exchange between the dual chambers by fitting observed GPS velocities to the Mogi source solutions to evaluate rates of volume change for the chambers (see *Elsworth et al.* [2008] for details). With volume fluxes defined in terms of dense rock equivalents (DRE), the effect of magma compressibility is accommodated by the compressibility factor, $C = 1 + 4G/3\beta_m$, where β_m is the bulk modulus of the magma [*Huppert and Woods*, 2002]; G, the shear modulus of the wallrock, is estimated on the basis of 1-D seismic velocity profile [*Shalev et al.*, 2010] and decreased by a factor of 10 to account for the large-strain effects and modulus "softening" [*Bonaccorso et al.*, 2005] that are unrepresented in the extrapolated 1-D seismic velocity data. The compressibility factor due to this modulus choice linearly affects the magma volumetrics of the shallow chamber but does not change our basic conclusion regarding the control of eruption.

4. Fit to Observations

[8] *Elsworth et al.* [2008] used pairs of GPS stations to individually solve for chamber inflation/deflation at depths prescribed a priori. Here we perform least squares fit inversions that search the full parameter space of potential chamber depths for a suite of up to 13 GPS stations available during 1995–2008. As with *Mattioli et al.* [2010], given the uncertainties involved (Figure 1, right), no statistic is robust enough to meaningfully constrain the depths of the chambers. With each source depth combination, we constrain the mass balance throughout the crustal column with the observed efflux. Thus the magma influx rate to the deep chamber (together with the chamber volumetrics) is calculated from the volume change rates of the chambers, in turn evaluated from geodetic inversions constrained for magma compressibility. In a volcanic system, the basal influx may be reasonably considered as constant over the timescale considered here [*Voight et al.*, 2010b]. The feasibility of this is examined by plotting the coefficient of variation of deep chamber influxes between six episodes of eruption or pause in the 1995–2008 time span (Figure 2, right).

[9] The (shallow, deep) chamber depth combinations (ca. 3–7.5, 13–22 km) have coefficients of variation for the deep influx less than 0.75, standard deviations between 0.41 to 1.19 m^3/sec and mean influx values of 0.88 to 1.69 m^3/sec. By constraining the shallow chamber centroid depth to 6–6.5 km (apparent depth 4.5–5 km) [*Barclay et al.*, 1998; *Voight et al.*, 2010a, 2010b], minimal coefficients of variation for the deep influx (Figure 2) arise for a deep chamber at about 15–21 km depth with a minimum at about 19 km resulting in a mean deep influx of 1.21 m^3/sec with a standard deviation of 0.47 m^3/sec during the six episodes of activation and pause. The standard variation of the deep influx remains under 0.60 m^3/sec for the deep chamber at 16–21 km and the shallow chamber at apparent depths 4–5.5 km (Figure 2, right). Least-squares inversions are then completed for average surface velocities for chambers fixed at 5 and 19 km depth.

[10] These inversions simultaneously satisfy (1) observed magma efflux rates, (2) conservation of magma mass within the crustal column, (3) compressibility conditions of the magma with depth, and (4) constant influx into the deep chamber. The details of the new inversion method will be the subject of a future publication. Geodetic results are shown in Figure 1 (right). Items (3) and (4) give significant extra constraint over previous results [*Elsworth et al.*, 2008] specifically in regard to polarity of chamber volume changes and identifying triggering mechanisms.

[11] Based on our analyses, constraining basal influx results in a slightly degraded fit to the data relative to the unconstrained case, but the difference is not significant as the changes in the coefficient of variation between the two sets are less than 5%. The benefit of adding this constraint,

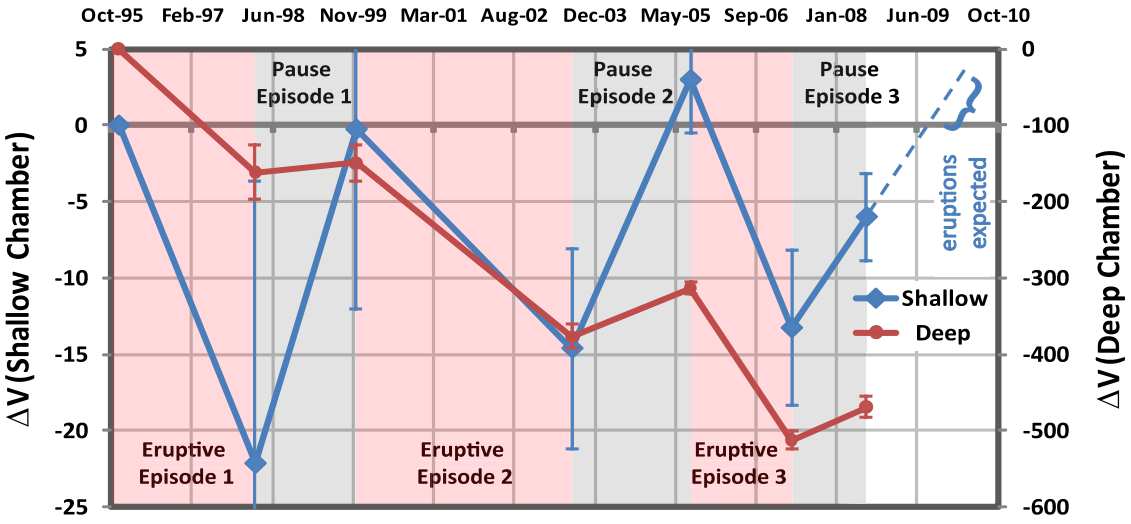

Figure 3. Cumulative volume changes of the deep (at 19 km: red) and shallow (at 5 km: blue) chambers (Mm^3) with error bars of one standard deviation. The dashed line indicates a projected shallow-chamber volume-change line potentially useful for forecasts, assuming that the magma system dynamics remains unchanged. However, the SHV system changed significantly after July 2008.

however, is that the resulting model satisfies the expectation that deep influx remain largely unperturbed by feedbacks from fluid transfer within the shallow crust in the decade-long time-scale considered here (i.e., that the magma supply rate driven by the subducting slab is uniform over long periods).

5. Implications for Eruption Periodicity

[12] The analysis enables cumulative volume changes of the deep and shallow magma chambers to be evaluated (Figure 3). Eruptive then pause episodes are characterized by synchronous deflation then inflation of both shallow and deep chambers. The depletion rate of the deep chamber exceeds its inflation rate, and has depleted ~500 Mm^3 in volume since the initiation of activity in 1995. The total erupted material (DRE) for the first 3 cycles is 950 Mm^3 implying that about half of the erupted material has been supplied from sources below the deep chamber.

[13] A consistent observation, repeated through three episodes, is that the eruptive episode starts approximately at the time that the shallow chamber has (re)gained its original volume after each preceding pause (Figure 3). Eruption is triggered as either the volume of the shallow chamber or its related internal pressure reaches a threshold magnitude and (re)fractures the chamber exit and thus allows magma to enter a conduit that connects to the ground surface [*Voight et al.*, 2010b]. Significantly, this observation can be used to predict the timing for the new activation phase.

[14] A complementary observation is that the eruptive phase transitions to a pause when the shallow chamber has lost 16–22 Mm^3 of its volume during the eruption (Figure 3). If this chamber volume change (avg. 18 Mm^3) is equivalent to a stress change limited by the hot tensile strength of intrusives, about 5–20 MPa [*Pinel and Jaupart*, 2003; *Tuffen and Dingwell*, 2004] then the size of the shallow magma chamber can be estimated. The tangential tensile stress around a pressurized sphere is half of its internal pressure, so the pressure (in excess of lithostatic) of the chamber at the onset of the eruption phase is 10–40 MPa. We assume static shear modulus in the range 3–10 GPa for the shallow crust surrounding the magma chamber (modulii based on island-wide 1-D tomography data to <5 km depth [*Shalev et al.*, 2010] are not reliable for this purpose because these data do not record the low seismic velocities of high temperature rock enclosing the SHV magma system). Knowing the average cyclic volume loss due to eruption (18 Mm^3), the pressure loss can be computed as a function of chamber radius. Capping the pressure loss to 40 MPa (maximum initial excess pressure), the chamber size cannot be smaller than ~1.8 km^3 for G = 3 GPa, or 6.0 km^3 for G = 10 GPa. Pressure losses in the range 10–20 MPa yield volumes 3.6 to 7.2 km^3 for G = 3 GPa, and volumes 12 to 24 km^3 for G = 10 GPa. Assuming a volume of 4 km^3 [*Voight et al.*, 2006], the pressure drop at the end of an eruption episode will be ~17 MPa for G = 3 GPa, and 57 MPa for G = 10 GPa, the latter seemingly excessive. The above calculations refer to the case for 40% crystallinity. For 60% volume crystal content, the average volume loss is 14 ± 3 Mm^3, yielding slightly reduced chamber dimensions. Interpreting these results, if we take pressure losses of 10–20 MPa as most likely, we find that chamber volumes >10 km^3 are only feasible if G > 10 GPa, whereas smaller chambers <10 km^3 require a low-modulus.

6. Summary

[15] Concurrent observations of surface efflux and surface deformation illuminate rates and patterns of magma transport at crustal depths below SHV. Our analysis uses a two-chamber model coupling fluid mass balance and surface-measured deformation with compressible magmatic constituents. We simultaneously invert geodetic data and measured magma efflux rates with the additional constraint of constant basal influx to determine rates of magma redistribution in the crust. Results constrain basal supply to be ~1.2 m^3/s for the recent activity (1995–2008). Volume changes within the deep and shallow chambers are synchronous but differ in modality as the larger deep chamber is net depleting with time while the

smaller upper chamber cycles between upper and lower limiting volumes – interpreted as limiting overpressures that either initiate or staunch the eruption. If limit overpressures are 10–20 MPa, shallow chamber volumes >10 km^3 are feasible if rock shear modulus is larger than 10 GPa; a small chamber <10 km^3 would require very low-modulus behavior. These observations provide rare direct evidence that volumetric thresholds and conjectured magma over- and under-pressures control the periodicity of eruptions in progress.

References

Annen, C., J. D. Blundy, and R. S. J. Sparks (2005), The genesis of intermediate and silicic magmas in deep crustal hot zones, *J. Petrol.*, *47*(3), 505–539, doi:10.1093/petrology/egi084.

Aspinall, W. P., A. D. Miller, L. L. Lynch, J. L. Latchman, R. C. Stewart, R. A. White, and J. A. Power (1998), Soufriere Hills eruption, Montserrat, 1995–1997: Volcanic earthquake locations and fault plane solutions, *Geophys. Res. Lett.*, *25*(18), 3397–3400, doi:10.1029/98GL00858.

Barclay, J., M. J. Rutherford, M. R. Carroll, M. D. Murphy, J. D. Devine, J. Gardner, and R. S. J. Sparks (1998), Experimental phase equilibria constraints on pre-eruptive storage conditions of the Soufriere Hills magma, *Geophys. Res. Lett.*, *25*(18), 3437–3440, doi:10.1029/98GL00856.

Bonaccorso, A., S. Cianetti, C. Giunchi, E. Trasatti, M. Bonafede, and E. Boschi (2005), Analytical and 3-D numerical modelling of Mt. Etna (Italy) volcano inflation, *Geophys. J. Int.*, *163*(2), 852–862, doi:10.1111/j.1365-246X.2005.02777.x.

Burnham, C. (1975), Water and magmas; a mixing model, *Geochim. Cosmochim. Acta*, *39*, 1077–1084, doi:10.1016/0016-7037(75)90050-2.

Costa, A., O. Melnik, R. S. J. Sparks, and B. Voight (2007), Control of magma flow in dykes on cyclic lava dome extrusion, *Geophys. Res. Lett.*, *34*, L02303, doi:10.1029/2006GL027466.

Devine, J. D., M. D. Murphy, M. J. Rutherford, J. Barclay, R. S. J. Sparks, M. R. Carroll, S. R. Young, and J. E. Gardner (1998), Petrologic evidence for pre-eruptive pressure-temperature conditions, and recent reheating, of andesitic magma erupting at the Soufriere Hills volcano, Montserrat, WI, *Geophys. Res. Lett.*, *25*(19), 3669–3672, doi:10.1029/98GL01330.

Devine, J. D., M. J. Rutherford, G. E. Norton, and S. R. Young (2003), Magma storage region processes inferred from geochemistry of Fe-Ti oxides in andesitic magma, Soufriere Hills volcano, Montserrat, WI, *J. Petrol.*, *44*(8), 1375–1400, doi:10.1093/petrology/44.8.1375.

Elsworth, D., G. Mattioli, J. Taron, B. Voight, and R. Herd (2008), Implications of magma transfer between multiple reservoirs on eruption cycling, *Science*, *322*(5899), 246–248, doi:10.1126/science.1161297.

Foroozan, R., D. Elsworth, B. Voight, and G. Mattioli (2010), Dual reservoir structure at Soufriere Hills Volcano inferred from continuous GPS observations and heterogeneous elastic modeling, *Geophys. Res. Lett.*, *37*, L00E12, doi:10.1029/2010GL042511.

Huppert, H. E., and A. W. Woods (2002), The role of volatiles in magma chamber dynamics, *Nature*, *420*(6915), 493–495, doi:10.1038/nature01211.

Loughlin, S. C., R. Luckett, G. Ryan, T. Christopher, V. Hards, S. De Angelis, L. Jones, and M. Strutt (2010), An overview of lava dome evolution, dome collapse and cyclicity at Soufrière Hills Volcano, Montserrat, 2005–2007, *Geophys. Res. Lett.*, *37*, L00E16, doi:10.1029/2010GL042547.

Mattioli, G. S., and R. Herd (2003), Correlation of cyclic surface deformation recorded by GPS geodesy with surface magma flux at Soufriere Hills volcano, Montserrat, *Seismol. Res. Lett.*, *74*(2), 230.

Mattioli, G., R. Herd, M. Strutt, G. Ryan, C. Widiwijayanti, and B. Voight (2010), Long term surface deformation of Soufriere Hills Volcano, Montserrat from GPS geodesy: Inferences from simple elastic inverse models, *Geophys. Res. Lett.*, *37*, L00E13, doi:10.1029/2009GL042268.

Melnik, O., and R. S. J. Sparks (1999), Nonlinear dynamics of lava dome extrusion, *Nature*, *402*(6757), 37–41, doi:10.1038/46950.

Miller, V., B. Voight, C. J. Ammon, E. Shalev, and G. Thompson (2010), Seismic expression of magma-induced crustal strains and localized fluid pressures during initial eruptive stages, Soufrière Hills Volcano, Montserrat, *Geophys. Res. Lett.*, *37*, L00E21, doi:10.1029/2010GL043997.

Mogi, K. (1958), Relations between the eruptions of various volcanoes and the deformations of the ground surfaces around them, *Bull. Earthquake Res. Inst. Univ. Tokyo*, *36*, 99–134.

Murphy, M. D., R. S. J. Sparks, J. Barclay, M. R. Carroll, and T. S. Brewer (2000), Remobilization of andesite magma by intrusion of mafic magma at the Soufriere Hills Volcano, Montserrat, West Indies, *J. Petrol.*, *41*(1), 21–42, doi:10.1093/petrology/41.1.21.

Pinel, V., and C. Jaupart (2003), Magma chamber behavior beneath a volcanic edifice, *J. Geophys. Res.*, *108*(B2), 2072, doi:10.1029/2002JB001751.

Shalev, E., et al. (2010), Three-dimensional seismic velocity tomography of Montserrat from the SEA-CALIPSO offshore/onshore experiment, *Geophys. Res. Lett.*, *37*, L00E17, doi:10.1029/2010GL042498.

Tuffen, H., and D. B. Dingwell (2004), Fault textures in volcanic conduits: Evidence for seismic trigger mechanisms during silicic eruptions, *Bull. Volcanol.*, *67*(4), 370–387, doi:10.1007/s00445-004-0383-5.

Voight, B., et al. (2006), Unprecedented pressure increase in deep magma reservoir triggered by lava-dome collapse, *Geophys. Res. Lett.*, *33*, L03312, doi:10.1029/2005GL024870.

Voight, B., et al. (2008), Conundrum on magmatic reservoir of Soufriere Hills Volcano, Montserrat: enigmatic evidence and the case for a vertically-elongated reservoir, *Eos Trans. AGU*, *89*(53), Fall Meet. Suppl., Abstract V53C-395.

Voight, B., et al. (2010a), Active source experiment peers under Soufriere Hills Volcano, *Eos Trans. AGU*, *91*(28), 245, doi:10.1029/2010EO280002.

Voight, B., C. Widiwijayanti, G. Mattioli, D. Elsworth, D. Hidayat, and M. Strutt (2010b), Magma-sponge hypothesis and stratovolcanoes: Case for a compressible reservoir and quasi-steady deep influx at Soufriere Hills Volcano, Montserrat, *Geophys. Res. Lett.*, *37*, L00E05, doi:10.1029/2009GL041732.

Wadge, G., R. Herd, G. Ryan, E. Calder, and J. Komorowski (2010), Lava production at Soufriere Hills Volcano, Montserrat: 1995–2009, *Geophys. Res. Lett.*, *37*, L00E03, doi:10.1029/2009GL041466.

D. Elsworth and R. Foroozan, Department of Energy and Environmental Engineering, G3 Center and EMS Energy Institute, Pennsylvania State University, 230 A Hosler Bldg., University Park, PA 16802, USA. (rzforoozan@gmail.com)

G. S. Mattioli, Department of Earth and Environmental Sciences, University of Texas at Arlington, Box 19049, Arlington, TX 76019-0049, USA.

B. Voight, Department of Geosciences, Pennsylvania State University, 503 Deike Bldg., University Park, PA 16802-2714, USA.